

Stellar Feedback and the Energy Budget of Late-Type Galaxies: Missing Baryons and Core Creation

Harley Katz^{1*}, Harry Desmond^{1†}, Federico Lelli^{2‡}, Stacy McGaugh³,
Arianna Di Cintio^{4,5}, Chris Brook^{4,5} and James Schombert⁶

¹*Astrophysics, University of Oxford, Denys Wilkinson Building, Keble Road, Oxford OX1 3RH, UK*

²*European Southern Observatory, Karl-Schwarzschild-Strasse 2, Garching bei Munchen, Germany*

³*Department of Astronomy, Case Western Reserve University, Cleveland, OH 44106, USA*

⁴*Instituto de Astrofísica de Canarias, Calle Via Láctea s/n, E-38206 La Laguna, Tenerife, Spain*

⁵*Universidad de La Laguna. Avda. Astrofísico Fco. Sánchez, La Laguna, Tenerife, Spain*

⁶*University of Oregon, Department of Physics, Eugene OR, 97403, USA*

6 August 2018

ABSTRACT

In a Λ CDM cosmology, galaxy formation is a globally inefficient process: it is often the case that far fewer baryons are observed in galaxy disks than expected from the cosmic baryon fraction. The location of these “missing baryons” is unclear. By fitting halo profiles to the rotation curves of galaxies in the SPARC data set, we measure the “missing baryon” mass for individual late-type systems. Assuming that haloes initially accrete the cosmological baryon fraction, we show that the maximum energy available from supernovae is typically not enough to completely eject these “missing baryons” from a halo, but it is often sufficient to heat them to the virial temperature. The energy available from supernovae has the same scaling with galaxy mass as the energy needed to heat or eject the “missing baryons”, indicating that the coupling efficiency of the feedback to the ISM may be constant with galaxy virial mass. We further find that the energy available from supernova feedback is always enough to convert a primordial cusp into a core and has magnitude consistent with what is required to heat the “missing baryons” to the virial temperature. Taking a census of the baryon content of galaxies with $10^9 < M_{\text{vir}}/M_{\odot} < 10^{12}$ reveals that $\sim 86\%$ of baryons are likely to be in a hot phase surrounding the galaxies and possibly observable in the X-ray, $\sim 7\%$ are in the form of cold gas, and $\sim 7\%$ are in stars.

Key words: galaxies: general, galaxies: formation, galaxies: evolution, galaxies: haloes, galaxies: spiral, galaxies: fundamental parameters

1 INTRODUCTION

In the early Universe, it is predicted that dark matter and baryons are well mixed (Spergel et al. 2003). As dark matter haloes form by gravitational collapse, the baryons cool, dissipate energy, and fall to the centres of the haloes (White & Rees 1978; Fall & Efstathiou 1980). Assuming a simple model where no other processes are at play, the total mass of a galaxy should then be composed of $\sim 15\%$ baryons and $\sim 85\%$ dark matter (Planck Collaboration et al. 2015). However, only in the most massive galaxy clusters does the observed baryon fraction begin to approach this value (Gio-

dini et al. 2009; Gonzalez et al. 2013), while at dwarf galaxy masses, only $\sim 1\%$ of the expected baryon content is actually detected (McGaugh et al. 2010; Papastergis et al. 2012; Bradford et al. 2015). A simple observational census of the baryonic content of the Universe therefore reveals that most baryons have not been identified.

Many of these “missing baryons” may reside in the inter-galactic medium (IGM), although this is unlikely to account for the full expected quantity (Fukugita et al. 1998; Danforth & Shull 2005; Shull et al. 2012). Alternatively, these “missing baryons” may exist in a phase that is difficult to detect (Bregman et al. 2015). Accretion onto dark matter haloes can shock heat the gas up to the virial temperature (T_{vir}), which would make the gas emit primarily in the X-ray (White & Frenk 1991; Cen & Ostriker 1999). Many hydrodynamic simulations show that galaxies, espe-

* E-mail: harley.katz@physics.ox.ac.uk

† St. John’s JRF

‡ ESO Fellow

cially at high redshift, are primarily fed by cold flows which penetrate deep into the centres of the haloes (Kereš et al. 2005). However, this may not be the case at low redshift. Strong feedback processes resulting from galaxy formation can reheat much of this gas into a hot phase, placing the primary emission in the X-ray (Mathews & Baker 1971; McKee & Ostriker 1977; Cen & Ostriker 1999). Hot gaseous haloes have been detected around a number of galaxies (Anderson & Bregman 2011; Anderson et al. 2013; Miller & Bregman 2015; Bregman et al. 2018), although for massive spirals, this may not completely account for the entire budget of “missing baryons” (Li et al. 2018; Bregman et al. 2018). Hot baryons may also be detected by the thermal Sunyaev-Zel’dovitch (kSZ) effect (de Graaff et al. 2017; Tanimura et al. 2017). As observations improve more of the “missing baryons” are being found, but it is unclear whether they are sufficient to make up the baryon content of the Universe.

This inefficiency by which galaxies either obtain or retain their baryons translates directly into the stellar content of galaxies. Abundance matching techniques predict that even for the most efficient star-forming galaxies, the fraction of stars present remains far below the cosmic baryon fraction at all masses (Moster et al. 2013; Behroozi et al. 2013; Moster et al. 2017). Explanations for the low fraction of stars come from feedback in three regimes. At the very lowest halo masses, ($M_{\text{halo}} \lesssim 10^9 M_{\odot}$), reionization may have completely prevented galaxies from forming by limiting their ability to accrete gas (Babul & Rees 1992; Efstathiou 1992; Gnedin 2000; Okamoto et al. 2008). At slightly higher masses, supernova (SN) feedback can limit star formation by either ejecting gas from the halo or keeping it at a temperature $T \sim T_{\text{vir}}$ (Dekel & Silk 1986). Finally, at the highest mass systems, feedback from AGN may be the dominant mechanism which regulates galaxies (Silk & Rees 1998; Bower et al. 2006).

Feedback processes can impact galaxies in many different ways. For example, the slope of the predicted black hole mass–stellar velocity dispersion relation depends on whether AGN outflows are “momentum-driven” or “energy-driven” (King 2003; Costa et al. 2014). For stellar feedback, the impulsiveness of the energy injection can determine whether or not a dark matter cusp can be converted into a core (Navarro et al. 1996a; Pontzen & Governato 2012). The way in which the feedback is modelled has drastic effects on observable quantities such as the stellar mass function and the galaxy distribution along the Hubble sequence (e.g. Schaye et al. 2015; Vogelsberger et al. 2014; Dubois et al. 2014; Hopkins et al. 2017), bulge formation (e.g. Hopkins et al. 2012), central black hole mass (e.g. Curtis & Sijacki 2016; Di Cintio et al. 2017), gas fractions and X-ray luminosities (e.g. Puchwein et al. 2008). Understanding the energy scales involved and how the feedback energy couples to the local medium is key to developing a complete model for galaxy formation.

Historically, one of the most well studied effects of feedback is how the density profile of the dark matter halo responds to large scale inflows or outflows of baryons (Navarro et al. 1996b; Pontzen & Governato 2012; Blumenthal et al. 1986; Gnedin et al. 2004; Katz et al. 2014; Martizzi et al. 2013; Read & Gilmore 2005; Read et al. 2016a). Peñarrubia et al. (2012) calculated the range of energies required to transform a cuspy density profile to one with a core and compared it to the energy budget of SN. They identified

that Milky Way dSphs require 10^{53-55} ergs of energy in order to form cores with sizes comparable to the luminous size of the galaxies. Using similar analytic reasoning, we focus here on how stellar feedback impacts the slope of the $M_{\star} - M_{\text{halo}}$ relation for late-type galaxies (spirals and dIrr) as well as dark matter density profiles.

We focus on two halo profiles: NFW (Navarro et al. 1996b), which is a prediction from cosmological DM-only simulations, and DC14 (Di Cintio et al. 2014b,a), which is a fit to the halos produced in the MaGICC simulations (Brook et al. 2012; Stinson et al. 2013) that include the effects of galaxy formation. This model includes a dependence of halo shape on $M_{\star}/M_{\text{halo}}$ such that the dark matter profiles of low and high mass galaxies are cuspy at the centre, while intermediate mass galaxies exhibit cores. Although this model is successful at accounting for the kinematics of a range of galaxy types (Di Cintio et al. 2014b; Katz et al. 2017) it is important to bear in mind that the formation of cores is a contentious issue among the current-generation of cosmological hydrodynamic simulations. For example, although other high-resolution simulations produce cores of roughly the DC14 type (e.g. Chan et al. 2015; Read et al. 2016b), others do not produce cores at all (e.g. Sawala et al. 2016). The exact mechanism of core formation has yet to be determined and there are indeed degeneracies in subgrid implementations of star formation and feedback that may lead to the same results. Nevertheless, since the DC14 model fits the properties of observed rotation curves well, we aim to use the energy scales of real galaxies as a further test of whether SN can provide enough energy to both regulate star formation and produce cores in real galaxies.

We begin by presenting observational results on the fraction of cold gas and stars of ~ 150 late-type galaxies from the SPARC data set (Lelli et al. 2016) (Sec. 2). We then review the theoretical motivation for how SN feedback regulates galaxy formation and show that in two simple models it naturally leads to a logarithmic slope of 5/3 for the $M_{\star} - M_{\text{vir}}$ relation (Sec. 3). These models are then tested against the SPARC data where this slope can be independently measured: we then check whether this energy budget is sufficient to generate a core in low mass galaxies or reverse adiabatic contraction in higher mass systems (Sec. 4). Finally, in Sec. 5 we use these results to take a cosmic census of the distribution of baryons in late-type galaxies with $10^9 < M_{\text{vir}} < 10^{12}$. Throughout this work, we assume a Λ CDM cosmology with $H_0 = 73 \text{ km s}^{-1} \text{ Mpc}^{-1}$, $\Omega_{\text{m}} = 0.24$, $\Omega_{\Lambda} = 0.76$, $\Omega_{\text{b}} = 0.04$ and $\sigma_8 = 0.76$ (Spergel et al. 2007), and we define the virial radius to be the radius which contains a mean density equal to $93.6 \rho_{\text{crit}}$.

2 OBSERVATIONAL CONSTRAINTS

2.1 SPARC Dataset and Rotation Curve Fitting

The SPARC sample¹ contains 175 galaxies with high quality rotation curves, interferometric observations at 21 cm, and baryon mass models from *Spitzer* [3.6 μm] photometry. We use this data to measure $f_{\text{d}} \equiv (M_{\text{gas,cold}} + M_{\star}) / ([\Omega_{\text{b}}/\Omega_{\text{m}}]M_{\text{vir}})$, the fraction of the galaxy

¹ astroweb.cwru.edu/SPARC/

mass that has settled into a cold disk, relative to the cosmological value, and $f_* \equiv M_*/(M_{\text{gas,cold}} + M_*)$, the fraction of baryons in stars. SPARC is ideal for this purpose as it contains late-type galaxies with a wide range of properties: $3 \times 10^7 \lesssim M_* (M_\odot) \lesssim 3 \times 10^{11}$, $20 \lesssim V_c \text{ (km/s)} \lesssim 300$, and $3 \lesssim \Sigma_* (M_\odot/\text{pc}^2) \lesssim 1500$. We extract from the SPARC data set a subsample of 147 galaxies which pass a series of selection criteria: 1) $i \geq 30^\circ$, 2) at least 5 observed rotation curve points, and 3) no major kinematic asymmetries between the approaching and receding sides of the disc (quality flag $Q < 3$).

We follow [Katz et al. \(2017\)](#) in fitting the rotation curves with either NFW or DC14 profiles. We fit these profiles using an MCMC algorithm with three free parameters: V_{vir} , c_{vir} and M_*/L where L is measured at $3.6\mu\text{m}$. We define a set of “flat” priors such that $10 < V_{\text{vir}} \text{ (km/s)} < 500$, $1 < c_{\text{vir}} < 100$, and $0.3 < M_*/L < 0.8$. The first two priors ensure that no walkers end up in extremely unphysical regimes. The prior on M_*/L is set to be consistent with [McGaugh & Schombert \(2014\)](#) who demonstrated that M_*/L shows no significant colour trends. [Katz et al. \(2017\)](#) demonstrated that the fitting results are rather robust to a variety of choices on M_*/L . Note that [Katz et al. \(2017\)](#) also fit each galaxy while assuming an additional set of “ Λ CDM” priors, where both the $M_{\text{halo}} - c$ and M_*/M_{halo} relations were imposed as lognormal priors on the fits. We do not include these priors here as we wish to constrain f_d and f_* from the data alone.

From the observations, we obtain the gas velocity, $V_{\text{cold,gas}}(r)$, stellar velocity (dependent on M_*/L), $V_*(r)$, and the circular velocity, $V_c(r)$. Hence

$$V_c^2(r) = V_{\text{cold,gas}}^2(r) + (M_*/L)V_*^2(r) + V_{\text{dark}}^2(r). \quad (1)$$

By fitting the rotation curves we constrain $V_{\text{dark}}^2(r) = V_{\text{hot,gas}}^2(r) + V_{\text{halo}}^2(r)$. $V_{\text{hot,gas}}^2(r) = 0$ corresponds to a feedback model where we assume that all unseen gas has been ejected from the halo. Alternatively, if we assume that the gas is heated to T_{vir} then it still resides in the halo and $V_{\text{hot,gas}}^2(r) \neq 0$. Given

$$M_{\text{vir}} = M_{\text{halo}} + M_* + M_{\text{gas,cold}} + M_{\text{gas,hot}}, \quad (2)$$

$$M_{\text{dark}} = M_{\text{halo}} + M_{\text{gas,hot}}, \quad (3)$$

and

$$M_{\text{halo}} = \frac{\Omega_{\text{DM}}}{\Omega_{\text{m}}} M_{\text{vir}} \quad (4)$$

we can separate the mass in hot gas from the dark matter component. We assume that the distribution of hot gas follows the same density profile as the dark matter. This is unlikely to be completely true as the hot gas probably has a higher concentration than the dark matter, although it is doubtful that introducing this additional freedom into the fitting would be fruitful. The difference between the models is subtle since $M_{\text{gas,hot}}$ is at most $\sim 20\%$ of the halo mass.

2.2 Estimating f_d and f_*

With the rotation curve fits in hand, we can now derive f_d and f_* directly from the observational data. In Figure 1, we

plot f_d as a function of M_{vir} . We fit these galaxies² with a linear model in log-space such that³

$$\log_{10}(f_d) = A \log_{10}(M_{\text{vir}}) + B. \quad (5)$$

In order to make these fits, we take into account the uncertainties on both M_{dark} and M_*/L that come from our MCMC fits. Unfortunately, the confidence intervals on our maximum posterior fits are both asymmetric and non-gaussian so we cannot perform an ordinary least square fit. Instead we adopt a bootstrap approach, as follows. First, we randomly choose a point in the 3D parameter space from 100,000 steps taken by the 100 walkers used in our MCMC chains, for each galaxy. We fit this resampled catalog with a RANSAC linear fitting algorithm ([Fischler & Bolles 1981](#); [Pedregosa et al. 2011](#)) in order to deal with potential outliers⁴. We repeat this procedure 10,000 times. The relation we quote is given by the mean of the fits to these catalogs, and the uncertainty in the fits is given by the standard deviation of the fitting parameters. Note that we only consider galaxies with $M_{\text{vir}} < 10^{13} M_\odot$ in our fits.

In Table 1, we list the fitting parameters measured from the data for Equation 5. It is clear that as the mass of the galaxy increases, so does the efficiency of cold disk formation. For the DC14 model, the evolution is rather weak and $f_d \propto M_{\text{vir}}^{0.16}$. There is still a reasonably large amount of scatter around this relation but the general trend persists. For the NFW model, the RANSAC algorithm finds a fit where the efficiency of disk formation also increases with galaxy mass. However there is so much scatter in this relation that the RANSAC algorithm classifies many of the points as outliers and this fit is not particularly trustworthy as there is no clear underlying relation. Within the uncertainties, the slopes of the DC14 and NFW relations are consistent. This is not particularly surprising since in certain regimes of M_*/M_{halo} , the DC14 model reduces to NFW. Outside of this regime, the DC14 model provides statistically better fits to the rotation curves than the NFW model ([Katz et al. 2017](#)): these galaxies are therefore outliers in the relation for the NFW model, driving our fitted relations closer to those of the DC14 model. These results agree with the $M_b - M_{\text{vir}}$ relation derived by combining the stellar mass abundance matching of [Moster et al. \(2013\)](#) with the $M_* - M_{\text{gas}}$ relation of [Dutton et al. \(2011\)](#).

Interestingly, the trend in f_d never comes close to unity, indicating that most of the baryons in late-type galaxies do not reside in cold disks, consistent with many other works in the literature ([Fukugita et al. 1998](#); [Danforth & Shull 2005](#); [Shull et al. 2012](#)). Rather, $f_d \ll 1$ implies that galaxy formation is a globally inefficient process.

Possible scenarios that may lead to $f_d < 1$ include: 1) the baryons never cooled and settled into a disk in the first place, or 2) the baryons settled into a disk and then feedback

² For all fits in this paper, we only consider galaxies with virial mass $< 10^{13} M_\odot$. We find similar results when fitting when using a maximum mass of $< 10^{12} M_\odot$.

³ The p -value of Pearson’s test on the $f_d - M_{\text{vir}}$ correlation for the DC14 model is 0.02, indicating a statistically significant linear relation.

⁴ The RANSAC algorithm is completely different from sigma clipping and uses an iterative method to robustly search the data set for inliers and outliers.

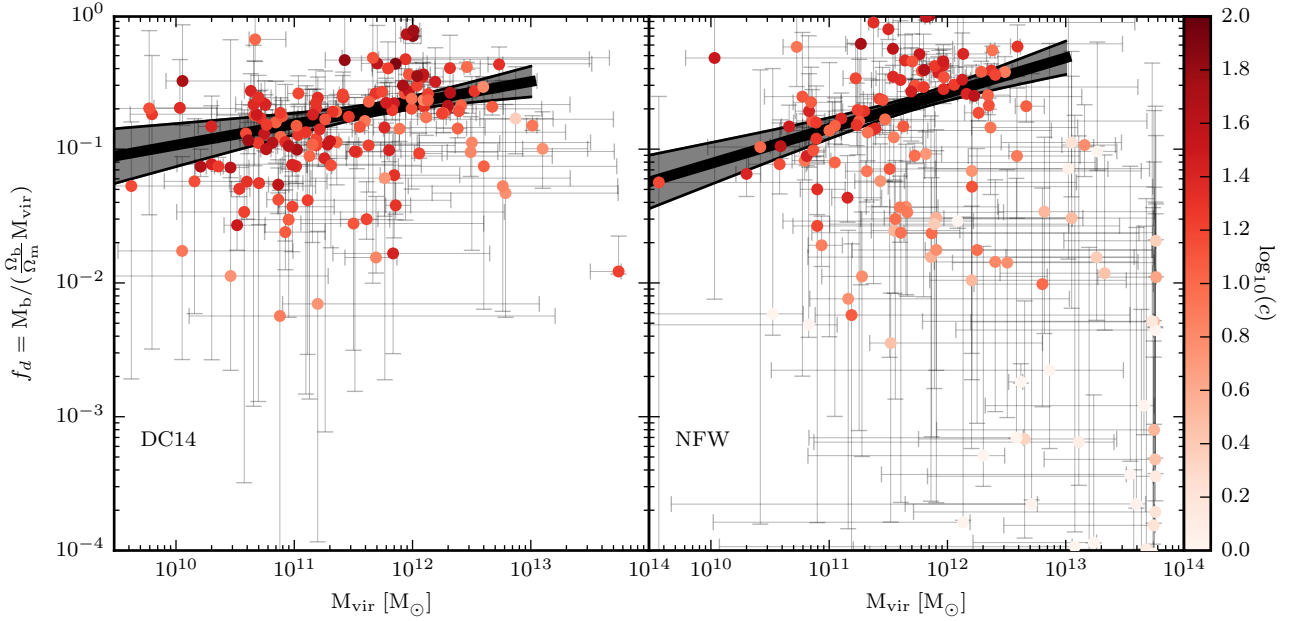


Figure 1. f_d as a function of the virial mass of the galaxy for the DC14 model (left) and the NFW model (right). The points represent the maximum likelihood fits to the observed rotation curves and they are coloured by the log of the concentration. The error bars represent the 2σ uncertainties on the parameters for individual galaxies. Note that the concentrations measured for the DC14 model are in much better agreement with the expected mass-concentration relation than for the NFW model [Katz et al. \(2017\)](#). The thick black line shows the best fit values to the function given in Equation 5 when the RANSAC algorithm is used, and the grey shaded region shows the 1σ uncertainty on this fit.

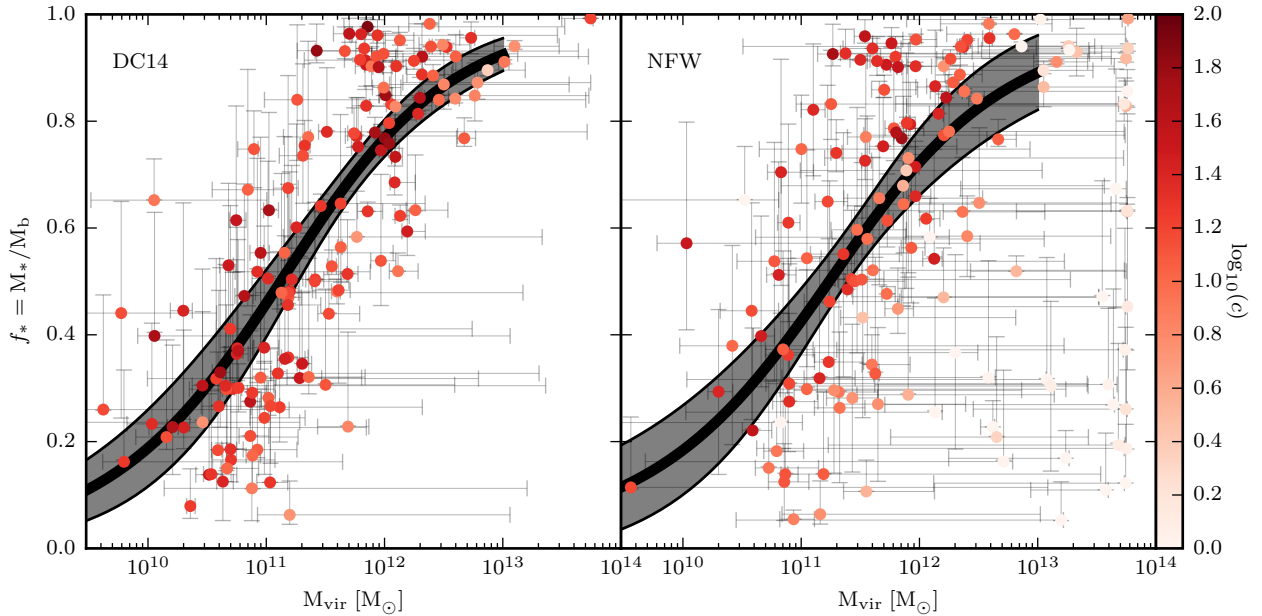


Figure 2. f_* as a function of M_{vir} for the DC14 model (left) and the NFW model (right). The points represent the maximum likelihood fits to the observed rotation curves and they are coloured by the log of the concentration. The error bars represent the 2σ uncertainties on the parameters for individual galaxies. The thick black line shows the best fit values to the function given in Equation 6 as determined by the RANSAC algorithm. The grey shaded region shows the 1σ uncertainty on this fit.

Halo Model	A	σ_A	B	σ_B	σ_{f_d}
DC14	0.16	0.09	-2.55	1.02	0.14 dex
NFW	0.26	0.09	-3.74	1.02	0.24 dex

Table 1. Fitting parameters for f_d as a function of M_{vir} as given in Equation 5 along with their uncertainties. σ_A and σ_B are the $1 - \sigma$ uncertainties on the slope and normalisation of relation calculated from the 10,000 RANSAC fits to the resampled catalogues. σ_{f_d} is the scatter in f_d calculated as 1.48 times the average median absolute deviation of the inliers of the 10,000 RANSAC fits.

processes heated them up or ejected them from the galaxy. Of course, these two scenarios are not mutually exclusive. There is evidence for galactic winds in many star forming galaxies (e.g. [Veilleux et al. 2005](#)) and the presence of metals in the CGM confirms a degree of recycling and ejection of gas from inside the galaxy (e.g. [Tumlinson et al. 2017](#)). Likewise the observation of hot halo gas surrounding galaxies indicates that there is a substantial heating process (e.g. [Anderson & Bregman 2011](#)), although this may be due to virial shocks. It is important to note however that significant controversy still remains about the ubiquity of winds in star-forming systems, with some studies finding little evidence for them ([Lelli et al. 2014](#); [Concas et al. 2017](#)). If the mechanism that we describe here is responsible for setting the cold baryon fractions of late-type galaxies, we would expect some observational signatures of gas motion, at least in the most massive systems.

For the lowest mass galaxies, $M_{\text{vir}} \sim 10^9 M_{\odot}$, the virial temperatures approach the temperature of ionized gas ($\sim 10,000$ K) and reionization may have prevented accretion of gas onto some of these galaxies ([Gnedin 2000](#); [Okamoto et al. 2008](#)). For more massive galaxies, this should not be an issue, although stellar and AGN feedback can still inhibit accretion onto a galaxy (e.g. [Mitchell et al. 2017](#)). In the remainder of this work we will assume the “worst-case” scenario where all baryons that could have accreted onto the galaxy have done so, and subsequent feedback processes are entirely responsible for heating the “missing baryons” into a hot halo or ejecting them from the galaxy. There are many effects which may prevent gas accreting onto a halo; we discuss this assumption further and the effect it has on the required feedback strength in Section 5.4.

In Figure 2, we plot f_* as a function of M_{vir} for both the DC14 and NFW halo models. DC14 haloes convert as low as 10% and up to 60% of their available baryons into stars at $M_{\text{vir}} \sim 10^{11} M_{\odot}$, and $\sim 50 - 100\%$ at $M_{\text{vir}} \sim 10^{12} M_{\odot}$. Note that the scatter about the relation is very large even though the general trend is an increasing f_* with virial mass. The galaxies with the lowest relative baryon content are also the most inefficient at forming stars. Once again, we see a similar trend for the NFW model, although the scatter is larger.

We fit the galaxy formation efficiency as a function of M_{vir} to a logistic function (sigmoid curve) of the form:

$$f_* = \frac{1}{1 + e^{-C \log_{10}(M_{\text{vir}}/M_0)}}. \quad (6)$$

We constrain both C , which controls the steepness of the interpolation, and M_0 , which is the point where the galaxy formation efficiency is 50%. The procedure for this fit is

Halo Model	C	σ_C	$\log_{10}(M_0)$	$\sigma_{\log_{10}(M_0)}$	σ_{f_*}
DC14	1.38	0.296	11.10	0.17	0.38
NFW	1.28	0.388	11.21	1.13	0.46

Table 2. Fitting parameters for f_* as a function of M_{vir} as given by Equation 6. σ_{f_*} is the scatter in f_* calculated as 1.48 times the average median absolute deviation of the 10,000 fits

exactly analogous to what was done for the $f_d - M_{\text{vir}}$ relation: we create 10,000 mock catalogs with both f_* and M_{vir} computed from the MCMC chains, and use the RANSAC algorithm to find the best-fitting logistic function. The fitting parameters reported in Table 2 are calculated as the means over the 10,000 fits, and the uncertainties are the 1σ deviations. In Figure 2 we show the derived relation and confidence intervals as the thick black line and grey shaded region respectively.

We find that M_0 and C are similar between the two different halo models, and that galaxies with $M_{\text{vir}} \sim 10^{11.1} M_{\odot}$ convert $\sim 50\%$ of available baryons into stars.

3 THEORETICAL FRAMEWORK

SN feedback can in principle impart both momentum and heat to the gas ([Taylor 1950](#); [Sedov 1959](#)), each of which can play a role in regulating galaxy growth. If the mechanical feedback is strong enough that gas clouds reach the escape velocity of the halo (V_{esc}), then, absent significant hydrodynamical drag from the ISM, the gas may be completely ejected from the halo. Unless the gas is re-accreted, it is then unable to undergo future star formation. Alternatively, instead of ejecting gas from the halo, SN feedback may simply heat it to near the virial temperature of the halo, where it can either bubble off of the galaxy or be recycled onto the disk ([Brook et al. 2014](#); [Christensen et al. 2016](#)). Both of these mechanisms likely play a part in regulating star formation.

We calculate the energy needed to eject the “missing baryons” from the galaxy (E_{ej}) or heat them to the virial temperature (E_{heat}) as a function of the halo mass of the galaxy (M_{halo}), as follows:

$$E_{\text{ej}} = \frac{1}{2} M_X V_{\text{esc}}^2. \quad (7)$$

and

$$E_{\text{heat}} = \frac{3}{2} M_X \frac{k_B (T_{\text{vir}} - T_{\text{ini}})}{\mu m_p}. \quad (8)$$

where M_X is the gas mass which we wish to heat or eject, T_{vir} is the virial temperature of the halo, $T_{\text{ini}} = 10,000$ K (100 K) is the initial temperature of ionized (neutral) gas, k_b is the Boltzmann constant, m_p is the proton mass, and $\mu = 0.59$ (1.22) is the mean molecular weight of the ionized (neutral) gas.

These equations are necessarily very simplified descriptions of gas ejection and heating; Equation 7 assumes that the gas cloud resides initially near the centre of the halo, that the halo is in the steady state and not formed hierarchically, that there are no energy losses, and that there is no hydrodynamical drag. While the former two effects would cause overestimation of the energy required for the gas to leave

the halo, the latter two would cause the converse. We therefore retain this form for simplicity. Similarly, Equation 8 is subject to vagaries in heat transport within the gas between the patch heated specifically by the SNe and the rest of the ISM. Our oversimplification may be most evident in the case of a cold metal-rich cloud moving at high speed through a hot corona: in this case the differences in metallicities and densities may cause cooling of the coronal gas by the Kelvin-Helmholtz instability (Marinacci et al. 2010). Nevertheless, we believe Equations 7 and 8 will give a reliable intuition into the energy scales required to regulate a galaxy.

We aim to apply this model to both the NFW and DC14 models, which are subsets of the more general (α, β, γ) profile. For this reason, we have derived a series of analytic expressions that allow for quick evaluation of various quantities for the (α, β, γ) density profile without requiring numerical integrals⁵. These can be found in Appendix A.

3.1 Heating or ejecting the baryons

We now turn to T_{vir} , given by

$$T_{\text{vir}} = (\mu m_p / 2k_B) V_{\text{vir}}^2. \quad (9)$$

If $T_{\text{vir}} \gg T_{\text{ini}}$, which is true for galaxies with $M_{\text{vir}} \gtrsim 2 \times 10^9 M_{\odot}$ if the gas is ionized and always true if the gas is neutral, then $E_{\text{heat}} \propto M_X M_{\text{vir}}^{2/3}$. If we plug in our scaling for V_{esc} , we also find that $E_{\text{ej}} \propto M_X M_{\text{vir}}^{2/3}$. Interestingly, the scaling is the same for both quantities. We can compare this to the energy available from SN feedback (E_{fb}) which is given by

$$E_{\text{fb}}(M_{\text{vir}}) = E_{\text{SN}} \epsilon_c f_{\text{SN}} f_d(M_{\text{vir}}) f_*(M_{\text{vir}}) \frac{\Omega_b}{\Omega_m} M_{\text{vir}}, \quad (10)$$

where $E_{\text{SN}} = 10^{51}$ ergs is the energy of an individual SN explosion, ϵ_c is the fraction of that energy that couples to the ISM and contributes to driving a wind, $f_{\text{SN}} \sim 0.01 M_{\odot}^{-1}$ is the number of SN explosions per unit solar mass (Salpeter 1955) and is dependent on the stellar IMF, $f_d(M_{\text{vir}})$ is the fraction of the mass of the galaxy with respect to the cosmological value that settles into a cold disk

$$f_d = (M_{\text{gas,cold}} + M_*) / ([\Omega_b / \Omega_m] M_{\text{vir}}), \quad (11)$$

and $f_*(M_{\text{halo}})$ is the fraction of baryons that are part of the disk and form stars

$$f_* = M_* / (M_{\text{gas,cold}} + M_*). \quad (12)$$

Thus

$$f_d f_* \frac{\Omega_b}{\Omega_m} M_{\text{vir}} = M_*. \quad (13)$$

A priori, both f_d and f_* are unknown and both E_{SN} and f_{SN} are expected to be constant⁶. For simplicity, we assume that the efficiency with which SN couple to the ISM (ϵ_c) is independent of galaxy mass. For SN feedback to be the dominant mechanism which regulates galaxies in the mass range $10^{12} \gtrsim M_{\text{vir}} \gtrsim 10^9 M_{\odot}$, one must have $M_* \propto M_X M_{\text{vir}}^{2/3}$.

⁵ See Dekel et al. (2017) for an alternative model which also avoids such integrals and provides reasonable fits to rotation curves.

⁶ This assumes that the stellar IMF is constant as a function of halo mass.

For our back-of-the-envelope calculation, the quantity M_X is well approximated as $M_X \sim M_b \sim (\Omega_b / \Omega_m) M_{\text{vir}}$, where $M_b = M_* + M_{\text{gas,cold}} + M_{\text{gas,hot}}$ is the baryonic mass of the galaxy. Substituting in for M_X and M_{vir} in our scaling relation, we find

$$M_* \propto M_{\text{vir}}^{5/3}, \quad (14)$$

assuming that all of the baryons are either heated to the virial temperature of the galaxy or completely ejected, solely due to SN feedback. What we have just derived is the theoretical slope of the M_*/M_{halo} relation assuming that SN feedback is the dominant mechanism which regulates galaxies, and that the majority of baryons are not in stars or cold gas. If higher mass galaxies have fewer missing baryons compared to low mass galaxies the slope will be less than 5/3, and vice versa.

4 COMPARISON WITH OBSERVATION

4.1 Individual Galaxies

With both f_d and f_* measured for 147 galaxies from the SPARC data set, along with their masses and concentrations derived in Katz et al. (2017), we can now compare E_{ej} , E_{heat} , and E_{fb} . In the top row of Figure 3, we plot the energy required to eject or heat the “missing baryons” for each individual galaxy in our sample and compare it to the energy available in SN feedback. Here, we show the case where $\epsilon_c = 1$ (i.e. that all SN energy contributes to ejecting or heating the gas). We caution however that this is the most optimistic case. Not only will some SN energy fail to be transformed into kinetic energy, but gas along the plane of the disk will be less likely to escape if the outflow is primarily perpendicular. Hydrodynamical models predict that this may result in ϵ_c values significantly less than unity (Rogers & Pittard 2013; Walch & Naab 2015; Gentry et al. 2017). In addition, we have assumed that all the supernova energy couples to the central regions of a halo to make a core. If this is not true the efficiency of the feedback for core formation will be reduced by a further factor. Since E_{fb} depends linearly on ϵ_c , it is trivial to transform our results to other values. In the bottom row of Figure 3 we show the ratios of $E_{\text{fb}}/E_{\text{heat}}$ and $E_{\text{fb}}/E_{\text{ej}}$ which gives insight into the exact values of ϵ_c needed to either eject or heat the missing baryons.

For the DC14 model, the scatter is relatively tight. There are a few outliers as expected, but many of these have large uncertainties on the halo fits (Katz et al. 2017). We expect variation for individual galaxies because galaxy properties such as disk size, metallicity, star formation history, merger history, and environment may cause deviations from our simple model. It is however promising that we find relatively good agreement between the scalings of E_{fb} and E_{heat} or E_{ej} and that the scatter for individual galaxies is not huge.

There is significantly more scatter for the NFW model than for DC14. In Figure 3, the points which represent E_{fb} are merely a rescaling of the M_*/M_{halo} relation presented in Katz et al. (2017), where it was shown that the scatter in this plane was too large for the NFW model to be consistent with observations. For the NFW model, the scatter in E_{ej}

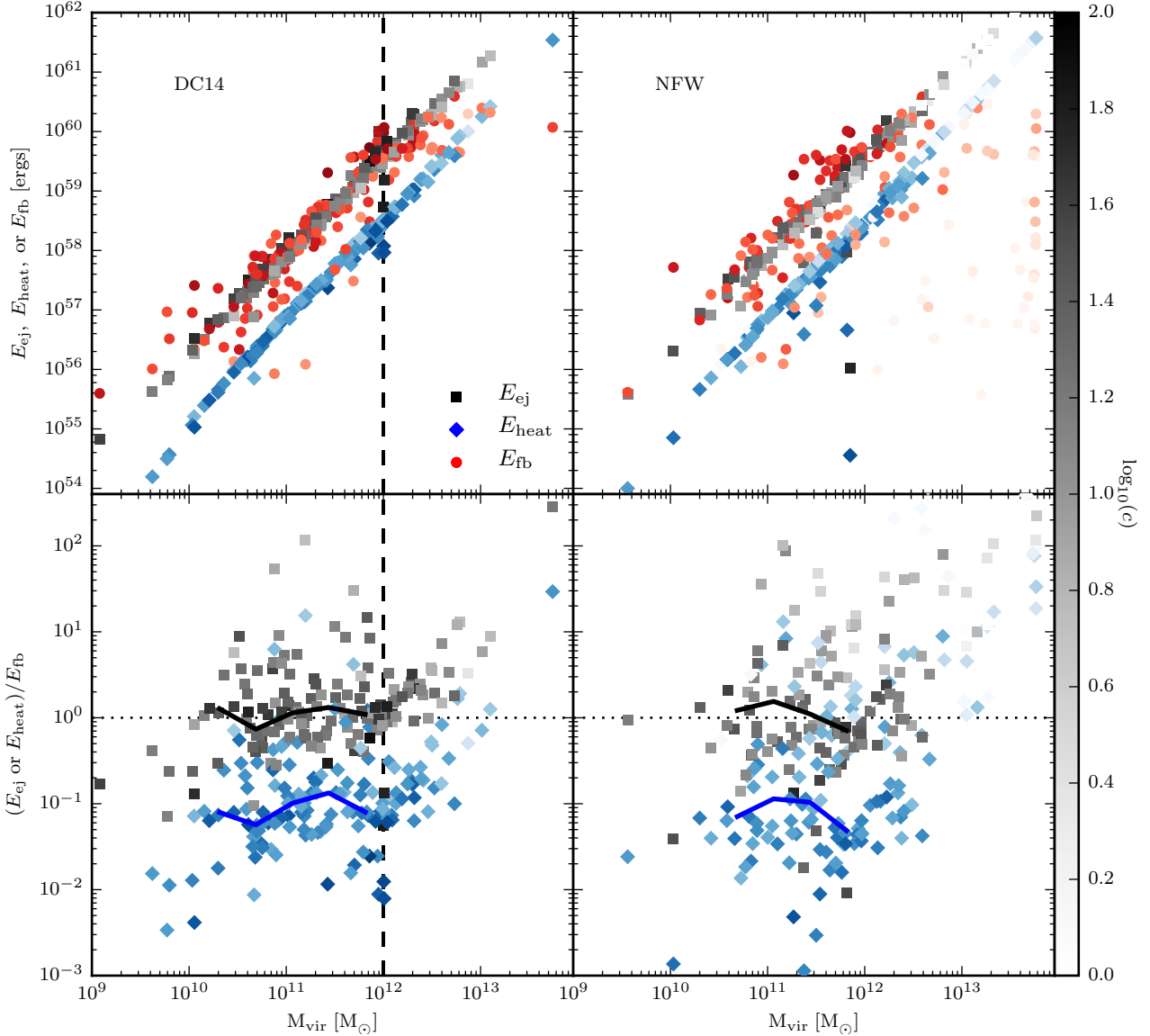


Figure 3. The top panel shows a comparison of energy available from SN, when all the energy is coupled to the ISM, i.e. $\epsilon_c = 1$ (red points), with the energy required to heat the “missing baryons” (blue points), or eject the “missing” baryons from the galaxy (black points) as a function of M_{vir} . The shading of the points is by the log of the concentration. The vertical dashed line represents the mass at which the DC14 model is expected to break down. The bottom panel shows the ratio of E_{ej} or E_{heat} to E_{fb} ; a value of 1 (shown the horizontal dotted line) indicates that SN energy is exactly sufficient to remove the gas or heat it to T_{vir} . The black and blue lines shows the median fraction of the SN energy that needs to couple to the gas (in bins of $\Delta \log_{10}(M_{\text{vir}}) = 0.375$ for systems with $M_{\text{vir}} < 10^{12} M_{\odot}$) in order to eject or heat the baryons to the virial temperature of the halo, respectively. Bins with fewer than five galaxies are not shown.

and E_{heat} are dependent on the scatter in c through V_{esc} and weakly dependent on the scatter in M_b since for the most part $M_{\text{vir}} \gg M_b$. The scatter in c is clearly smaller than the scatter in M_* which is why there is much more observed scatter in E_{fb} for the NFW model compared to the scatter in E_{ej} and E_{heat} . This is not true for the DC14 model where the scatter in M_* is much smaller.

Looking at galaxies with $M_{\text{vir}} > 10^{12} M_{\odot}$ which corresponds to stellar mass just under $10^{11} M_{\odot}$, there is very tentative evidence for a slight turnover in the energy available from SN feedback while the energy needed to eject or heat the “missing baryons” continues to increase. At these

masses, we are using an extrapolation of the DC14 model so our interpretation needs to be taken with caution. This would however be consistent with the idea that at these masses other feedback mechanisms are starting to play a role (Schaye et al. 2015). This picture is in line with the observed luminosity function where we see a turnover in the slope at these masses (Li & White 2009; Bernardi et al. 2013).

Since the red points overlap the black points in the left panel of Figure 3, 100% of the energy available from SN would need to couple to the gas in order to eject all of the “missing baryons” from the halo. This value is rather unrealistic as it is well established that this coupling is inefficient

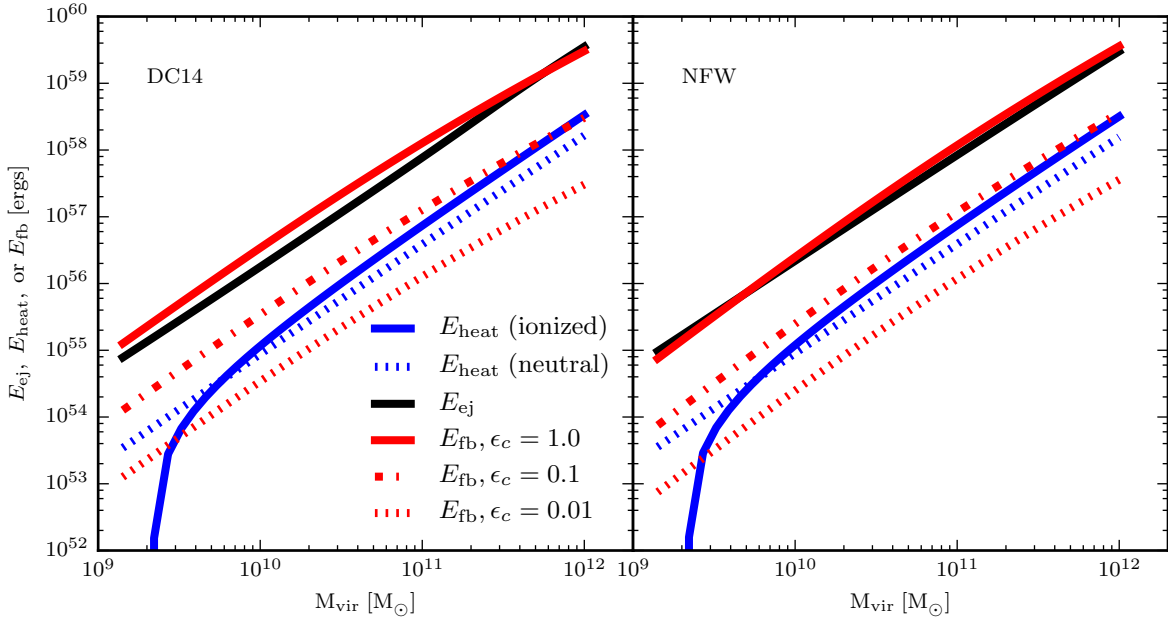


Figure 4. Comparison of energy available from SN feedback (red lines) with the energy required to heat the “missing” baryons (blue), or eject the “missing” baryons from the galaxy (black) as a function of M_{vir} . The different line styles for the red lines represent different coupling efficiencies of the SN energy to the ISM. The different line styles for the blue lines represent if the gas starts out ionized or neutral.

(Walch & Naab 2015; Rogers & Pittard 2013) and dependent on the density of the ambient medium (Cowie et al. 1981). As has been shown before (e.g. Yepes et al. 1997; Efsthathiou 2000), more energy is required to eject the “missing baryons” from the galaxy than to heat them to T_{vir} . Less than $\sim 10\%$ of the SN feedback energy needs to couple to the ISM in order to heat the gas to the virial temperature and have the red points overlap the blue points in the left panel of Figure 3. This value is strongly degenerate with the chosen stellar IMF: for more top heavy IMFs such as Chabrier (Chabrier 2003) the required coupling would be less than the value derived here. Nevertheless, it is likely that more of the “missing baryons” are located in a hot halo surrounding the galaxy than that they were ejected, even for our lowest mass systems of $\sim 10^9 M_{\odot}$. The key aspect of this diagram is that the slope of the red points is consistent with the slope of the black and blue points indicating that the amount of feedback energy available is a simple rescaling of the amount needed to heat or eject the “missing baryons”. This can be seen in the bottom panels of Figure 3 where we plot the median coupling efficiency, in bins of halo mass between $10^{10} < M_{\text{vir}}/M_{\odot} < 10^{12}$, required to heat or eject the “missing baryons”. This value is roughly constant as a function of halo mass. At lower masses, there are few galaxies in our sample and thus the median may not be truly representative. If SN are the dominant feedback mechanism regulating the galaxies, our work suggests that the coupling efficiency is constant across a wide range of halo masses.

In summary, even with 100% coupling efficiency of SN energy, there is often not enough energy to eject all of the “missing baryons” from the galaxy. For the DC14 model, only $\sim 9\%$ of the total energy available from SN needs to couple to the gas to heat it to the virial temperature of the

halo. We find that this value is reasonably independent of halo mass. We remind the reader however that our model is idealised: we have assumed that galaxies initially accrete the cosmological baryon fraction, all supernova energy couples with constant efficiency to dark matter in the central regions, and that halos begin with an NFW profile. More detailed conclusions will require hydrodynamical simulations where these assumptions are not necessary.

4.2 Mean Relations

Rather than perform this exercise for individual galaxies, we can use the mean relations for f_d and f_* derived in Section 2. In Figure 4, we plot the energy needed to either heat the “missing baryons” or eject them completely from the halo for both the DC14 and NFW models, and compare this to the energy available in SN feedback for three different constant values of ϵ_c . The mass in “missing baryons” is simply

$$M_X = (1 - f_d) \frac{\Omega_b}{\Omega_m} M_{\text{vir}}. \quad (15)$$

To calculate E_{ej} , we assume that all galaxies lie on the $M_{\text{halo}} - c$ relation as given in Dutton & Macciò (2014). Furthermore, to calculate V_{esc} for the DC14 model, we need to know α , β , and γ which can make up to $\sim 7\%$ difference in this velocity (see Figure A1). These can be determined from our fits of f_d and f_* , given the scaling relations presented in DC14. We plot two different quantities for E_{heat} , one assuming that the gas which is being heated starts out ionized ($T_{\text{ini}} = 10,000$ K and $\mu = 0.59$), and the other that the gas begins neutral ($T_{\text{ini}} = 100$ K and $\mu = 1.22$).

Figure 4 shows that E_{fb} , E_{ej} and E_{heat} scale in the same way with M_{vir} for both the DC14 and NFW models. The re-

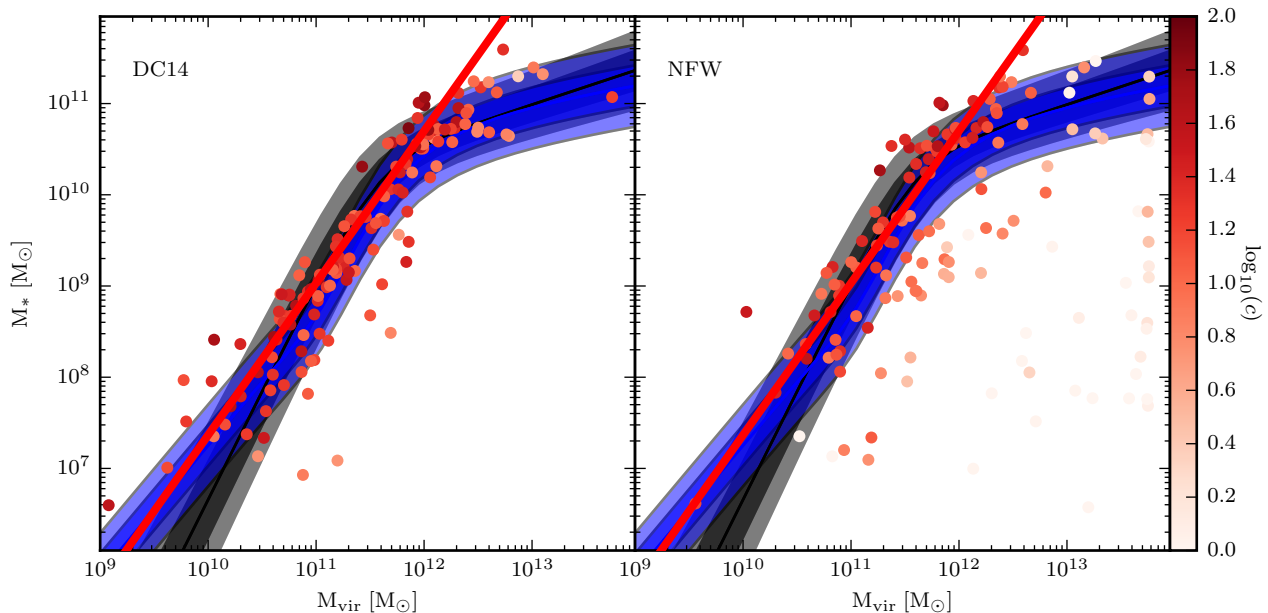


Figure 5. M_*/M_{halo} relation of the maximum posterior fits for each individual galaxy in our sample compared to the predicted relation from [Moster et al. \(2013\)](#) (grey shaded region) and [Behroozi et al. \(2013\)](#) (blue shaded region). The shaded regions map out the 1σ and 2σ scatter in the relations. Points are coloured by $\log_{10}(c)$. The red line shows an arbitrary scaling of $M_* \propto M_{\text{vir}}^{5/3}$. For $M_{\text{vir}} > 10^{12} M_{\odot}$, the $5/3$ scaling no longer well represents the data which may indicate that other processes, such as AGN, might be affecting these galaxies.

lation between f_d and M_{vir} has a large scatter and for the NFW model, it is not clear that the function we have fit to the data is truly representative. This likely stems from the fact that the NFW halo profile does not provide good fits to the rotation curves of SPARC galaxies ([Katz et al. 2017](#)), and therefore it is unwise to draw strong conclusions about the NFW halo from these mean relations. For the DC14 model, there is a much clearer indication that f_d increases with M_{vir} , and that the slope is roughly linear in log-space. It is encouraging that the DC14 model naturally predicts the scaling one would expect if SN feedback is the dominant mechanism regulating star formation and gas cooling in galaxies.

4.3 Comparison to other M_*/M_{halo} relations

In [Katz et al. \(2017\)](#), it was claimed that the maximum-likelihood parameters for the DC14 halo model fits adhered well to the M_*/M_{halo} relation predicted by [Moster et al. \(2013\)](#), even without Λ CDM priors. For the mass range we consider here ($10^{12} \gtrsim M_{\text{vir}}/M_{\odot} \gtrsim 10^9$), [Moster et al. \(2013\)](#) find $M_* \propto M_{\text{halo}}^{2.376}$. This scaling is clearly different to the relation of $M_* \propto M_{\text{halo}}^{5/3}$ predicted for galaxy regulation by SN. How then can our results be consistent with both?

In [Figure 5](#), we plot the M_*/M_{halo} relation of the maximum-likelihood fits from each galaxy in our sample compared to the predicted relations from [Moster et al. \(2013\)](#) and [Behroozi et al. \(2013\)](#). As was shown in [Katz et al. \(2017\)](#) the fits for the DC14 model adhere reasonably well to the 2σ scatter in the relation from [Moster et al. \(2013\)](#). Overplotted on this diagram is a red line with a scal-

ing of $M_* \propto M_{\text{vir}}^{5/3}$ and an arbitrary normalisation. Note that this is not a fit to the data. It is clear that the M_*/M_{halo} predicted by [Moster et al. \(2013\)](#) is slightly steeper than this relation, although within 2σ they are not in terrible disagreement. Although we find a different slope, we maintain approximate agreement with both relations.

The M_*/M_{halo} relation of [Behroozi et al. \(2013\)](#) is shallower at the low-mass end than [Moster et al. \(2013\)](#) and is therefore in better agreement with our predicted slope. Our normalisations tend to be slightly higher than [Behroozi et al. \(2013\)](#), although the disagreement is marginal at best. We should note however that their stellar masses are derived in a different band than the SPARC galaxies. There is a much larger uncertainty in M_*/L in visual bands than at 3.6μ ([McGaugh & Schombert 2014](#)) and there can be systematic differences between bands. Any disagreement between the normalisation of the DC14 model and these relations is marginal and can be readily reconciled with a change in M_*/L . Finally, the relations derived by [Behroozi et al. \(2013\)](#) and [Moster et al. \(2013\)](#) consider all galaxies, whilst we consider only late-type galaxies. Part of the difference in slope may well derive from morphological selection effects.

If we measure the slope of the $\log_{10}(M_*) - \log_{10}(M_{\text{vir}})$ relation directly from the data for systems with $M_{\text{vir}} < 10^{12} M_{\odot}$, we find this value to be 1.51 ± 0.13 for the DC14 model and 1.67 ± 0.20 for the NFW model. As expected, the slope is slightly less than $5/3$ for DC14 because there is a weak scaling of f_d with galaxy mass. For the NFW case the slope is $5/3$, albeit with a significant number of outliers. Note that “preventative feedback” which is biased towards low mass galaxies (e.g. radiative feedback from reion-

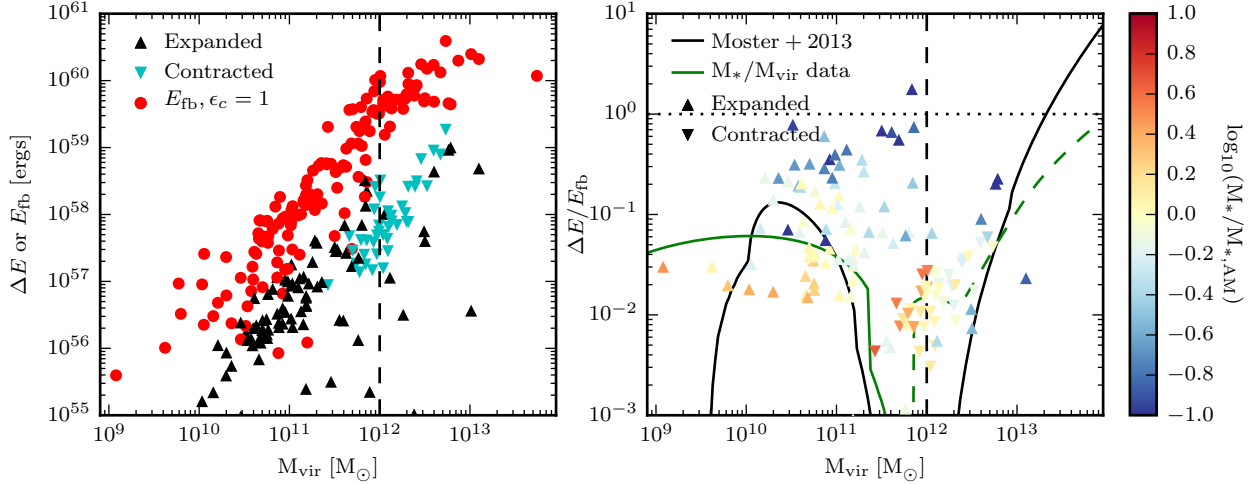


Figure 6. (Left) Energy needed to transform the halo from NFW to DC14 (black and cyan) versus the energy available in feedback (red). Black points represent that this process requires energy (i.e. that the DC14 model has removed mass from the centre compared to the primordial NFW halo) while cyan points represent contracted haloes and thus the energy difference is negative (i.e. mass has moved closer to the halo centre). The available feedback energy is shown for $\epsilon_c = 1$. (Right) The ratio of the energy needed to restructure the halo to the maximum energy available from SN. Upwards and downwards triangles represent cored and adiabatically contracted haloes, respectively. Galaxies falling below the dotted line have enough SN energy to either form a core or counter-balance adiabatic contraction. Points are color-coded by the logarithmic distance from the empirically determined $M_* - M_{vir}$ relation. Red points have higher than average stellar mass while blue points have lower than average stellar mass. The solid black line shows the expectation for galaxies that fall on the $M_* - M_{vir}$ relation and the $M_{vir} - c_{vir}$ relation from [Moster et al. \(2013\)](#) and [Macciò et al. \(2008\)](#), respectively. The green line is the same as the black line but considers the empirically determined $M_* - M_{vir}$ and $M_{vir} - c_{vir}$ relations from halo fits to the SPARC rotation curves. The solid and dashed portions of these curves indicates halos that have been expanded and contracted, respectively. Galaxies that follow the $M_* - M_{vir}$ relation from [Moster et al. \(2013\)](#) and the $M_{vir} - c_{vir}$ relation from [Macciò et al. \(2008\)](#) should always exhibit some degree of central expansion.

ization) would lead to an f_d scaling that would also cause the slope of this relation to become shallower than $5/3$.

5 DISCUSSION

5.1 The effect of cooling

It is clear from the previous section that there is not enough energy to eject all of the “missing baryons” out of the galaxy. If the gas is only heated to T_{vir} and remains in the halo, it has a chance to cool and settle back onto the disk. The simulations of [Christensen et al. \(2016\)](#) find that $\sim 50\%$ of material kicked out of the cold disk due to SN feedback is re-accreted on a timescale of ~ 1 Gyr, independent of halo mass. This would imply that in order to maintain the gas at the virial temperature of the halo, one would have to couple 50% more energy than we concluded from Equation 8.

For our individual galaxies, a coupling efficiency of $\sim 9\%$ is roughly what is required to heat all of the “missing baryons” to T_{vir} . To maintain this temperature if cooling is included, one would then require $\sim 13.5\%$ (assuming 50% of the baryons are re-accreted) of the total available energy from SN to couple thermally to the ISM. Once again, this is degenerate with the choice of stellar IMF. Assuming a Chabrier IMF ([Chabrier et al. 2005](#)) would decrease this value by a further $\sim 20\%$. This of course neglects any energy input pre-SN which may come in the form of stellar winds, radiation pressure, or photoheating of species other than hydrogen. Likewise, cosmic rays created in SN may play a role

in driving an outflow (e.g. [Breitschwerdt et al. 1991](#)). Furthermore, our estimates here are the absolute upper limits of the amount of energy one needs to account for the “missing baryons” as they assume that all baryons which should be in the halo have, at one point, accreted onto the cold disk. As has been shown from cosmological hydrodynamics simulations, the feedback energy can eject baryons as well as prevent accretion onto the halo which would reduce the amount of energy needed (e.g. [Mitchell et al. 2017](#)). For the more massive haloes, we may expect strong virial shocks. The actual amount of baryons that actually cool onto the disk is likely to be closer to 50% , independent of halo mass ([Christensen et al. 2016](#)), bringing our absolute upper limit for the net ϵ_c back down to $\sim 9\%$ if cooling is considered. It is well known that radiative cooling is a very efficient processes, making the coupling of thermal energy relatively inefficient. Our upper limit of $\epsilon_c \sim 9\%$ puts our model in the realistic regime of what can be expected from simulations (e.g. [Walch & Naab 2015](#); [Gentry et al. 2017](#)).

5.2 Energy needed to restructure the halo

Thus far, we have only been concerned with the energy required to remove the “missing baryons” from the centres of their host haloes. If we believe that the primordial haloes for these galaxies have NFW profiles, similar to [Peñarrubia et al. \(2012\)](#), we can calculate the change in gravitational

potential energy needed to convert them to a DC14 profile:

$$\Delta E = \frac{W_{\text{DC14}} - W_{\text{NFW}}}{2}, \quad (16)$$

where

$$W = -4\pi G \int_0^{R_{\text{max}}} \rho(r)M(r)rdr. \quad (17)$$

In the low mass regime, DC14 reverts back to NFW so $\Delta E = 0$. At high masses, adiabatic contraction is expected to be the dominant effect, resulting in $\Delta E < 0$. It is only at intermediate masses, between $10^6 < M_*/M_\odot < 10^{10}$, where the inner slope is shallower than -1 , that we expect mass to have been removed from the centre of the galaxy and hence $\Delta E > 0$. Peñarrubia et al. (2012) have set $R_{\text{max}} = R_{\text{vir}}$ as the upper bound for the integral in Equation 17. Maxwell et al. (2015) have pointed out that the upper bound for this integral should be set by a condition where both the mass and the density are equal between the two different halo density profiles. There is no generic radius where this is true when comparing DC14 to NFW and thus we have chosen the radius where the mass profiles first converge. Integrating out to R_{vir} does not change our results substantially and using our current method, we find that our results are consistent with both Maxwell et al. (2015); Brook & Di Cintio (2015).

In Figure 6, we use the DC14 model fits to calculate ΔE , and compare with the available energy from SN feedback assuming $\epsilon_c = 1$. Nearly all of the red points fall above the black points indicating that there is more energy available in the form of energetic feedback than is required to transform the halo. This can more easily be seen in the right panel of Figure 6 where we show the ratio of SN energy to the amount required to restructure the halo. At higher masses, adiabatic contraction takes over and ΔE becomes negative. The points in the right panel have been colored by the ratio of their stellar mass to the empirically determined $M_* - M_{\text{vir}}$ relation. The points that scatter high tend to have stellar masses that are lower than average, while the red points tend to fall lower and have higher than average stellar masses.

For the systems that exhibit cores, we find no mass strong dependence in the ratio of $\Delta E/E_{\text{fb}}$. The green curve is mostly flat between $10^9 < M_{\text{vir}}/M_\odot < 3 \times 10^{11}$. A median (IMF dependent) coupling efficiency of $\sim 5\%$ is required for SN to be the dominant mechanism driving core formation. There is once again significant scatter; however, this value is very consistent with the coupling efficiency that was obtained earlier when measuring how much energy was required to heat the “missing baryons” to the virial temperature of the halo. The ΔE that we require to create cores is in good agreement with what is found in Maxwell et al. (2015) for their larger core models (see their Figure 3). Note that our choice of R_{max} is often much larger than what is chosen in Maxwell et al. (2015) and hence we can expect to require slightly more energy. However, most of our systems do not exhibit central density slopes that are exactly zero and thus our energy requirement is lessened compared with the density profiles used in Maxwell et al. (2015) and thus we find a reasonable agreement.

Interestingly, the maximum energy available from SN is always greater than the energy loss during contraction. If the SN energy couples efficiently to the gas at a constant ϵ_c , as suggested earlier, one may wonder how contraction

is possible for such systems. For this, we must understand how the dark matter responds to changes in the potential. Pontzen & Governato (2012) have shown that transformations of the dark matter halo require non-adiabatic changes in the potential, which depends on the star formation history. For instance, a galaxy that formed all of its stars in a single burst is likely to have a larger core than a galaxy with a similar stellar and halo mass but a more protracted star formation history. It is well established that the specific star formation rate scales with stellar mass such that low mass galaxies have higher sSFRs compared to higher mass galaxies (e.g. Elbaz et al. 2007; Karim et al. 2011). Furthermore, simulations show that lower mass galaxies tend to have more bursty star formation histories compared to more massive galaxies (e.g. Brook et al. 2012). In the sample of galaxies presented here, a larger fraction of the higher mass galaxies exhibit contraction compared to lower mass systems which is consistent with this argument. However, Peñarrubia et al. (2012) have shown that the transformation is degenerate with formation redshift and other galaxy properties which may complicate our interpretation.

In contrast to the cored galaxies, we find a mass dependence in the ratio of $\Delta E/E_{\text{fb}}$ for the contracted systems such that $|\Delta E|/E_{\text{fb}} \propto M_{\text{vir}}^{0.9}$. This indicates that more massive systems require a higher coupling efficiency in order to erase the contraction compared to lower mass systems. The coupling efficiencies required to erase the contraction are rather low compared to what is required to create a core. All contracted systems require a coupling efficiency $< 10\%$ to erase the contraction. Although there is always enough energy available from SN to complete this transformation, it remains to be determined how efficiently that energy eventually couples to the dark matter as a function of halo mass for these contracted systems.

5.3 Where are the baryons?

Having formulae for f_d and f_* as functions of M_{vir} allows us to take a census of the baryons in late type galaxies in various phases. We have shown in Figure 4 that it is unlikely that the “missing baryons” have all been ejected from the haloes, but it is likely that many are in the hot phase surrounding galaxies. The fractional abundances of hot gas ($f_{\text{M}_{\text{gas,hot}}}$), cold gas ($f_{\text{M}_{\text{gas,cold}}}$), and stars (f_{M_*}) in the mass range $10^9 < M_{\text{vir}}/M_\odot < 10^{12}$ can be calculated as follows:

$$f_{\text{M}_{\text{gas,hot}}} = \frac{\int_{10^9 M_\odot}^{10^{12} M_\odot} (1 - f_d(M)) M \frac{dn}{dM}(M) dM}{\int_{10^9 M_\odot}^{10^{12} M_\odot} M \frac{dn}{dM}(M) dM}, \quad (18)$$

$$f_{\text{M}_{\text{gas,cold}}} = \frac{\int_{10^9 M_\odot}^{10^{12} M_\odot} f_d(M) M \frac{dn}{dM}(M) dM}{\int_{10^9 M_\odot}^{10^{12} M_\odot} M \frac{dn}{dM}(M) dM} - f_{\text{M}_*} \quad (19)$$

and

$$f_{\text{M}_*} = \frac{\int_{10^9 M_\odot}^{10^{12} M_\odot} f_*(M) f_d(M) M \frac{dn}{dM}(M) dM}{\int_{10^9 M_\odot}^{10^{12} M_\odot} M \frac{dn}{dM}(M) dM}, \quad (20)$$

where $\frac{dn}{dM}(M)$ is the mass function of dark matter haloes for late-type galaxies. In this case only the slope of the halo mass

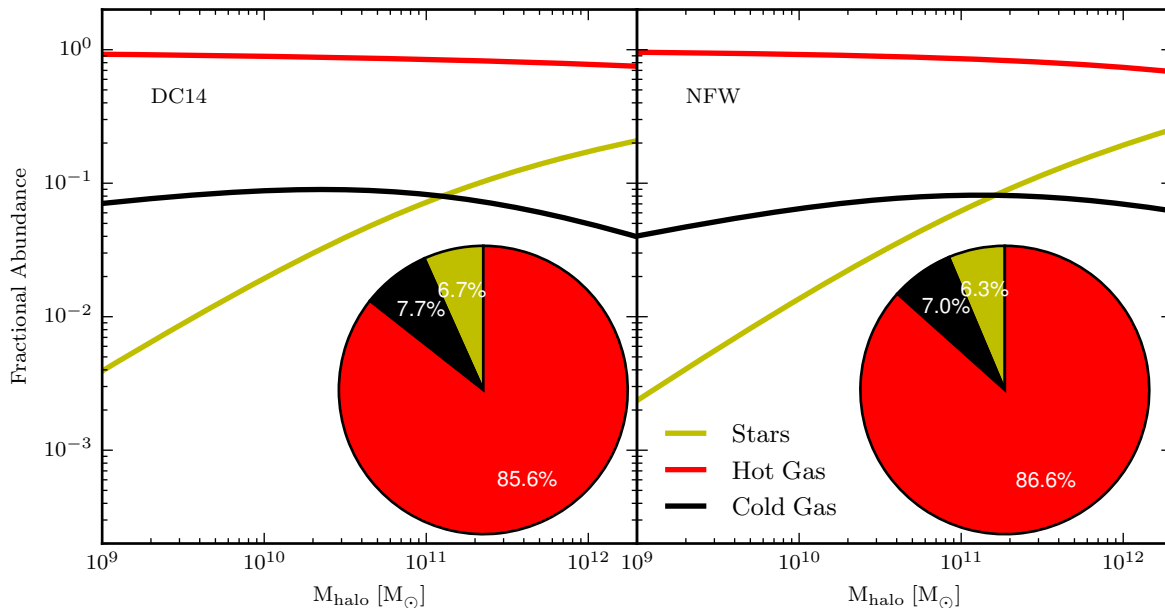


Figure 7. Fraction of cold gas (black), hot gas (red) and stars (yellow) as a function of M_{halo} . The inset pie charts show the fractional abundances integrated over the halo mass function.

function matters, and we assume this to be independent of the morphology of the central galaxy.

In Figure 7, we use these formulae to plot the fractional abundances of the three baryon phases as a function of halo mass. For this calculation, we have used the halo mass function for WMAP3 cosmology⁷ (Spergel et al. 2007). Over the entire mass range, $\sim 85\%$ of the gas is expected to be in the hot phase, $\sim 7 - 8\%$ of the total gas is in the cold phase, and $\sim 6 - 7\%$ in stars. At least over this mass range, galaxy formation is therefore extremely inefficient: only $\sim 13 - 15\%$ of the baryons exist as cold gas or stars.

As the mass of the halo increases, so does the fraction of the total baryons in stars. For the DC14 models, the fraction of cold gas remains relatively constant as a function of halo mass and has a peak of $\sim 8\%$ at $M_{\text{halo}} \sim 6 - 8 \times 10^{10} M_{\odot}$. The NFW model exhibits a similar amplitude peak for the cold gas mass fraction, although this occurs at a marginally higher halo mass. These curves may be used to constrain feedback models in simulations: not only should such models produce the right amount of stars, they should also give the correct proportion of cold gas. Although one would expect a significant amount of galaxy-to-galaxy scatter (visible in Figures 1 and 2), these baryon phase relations should be obtained on average over the galaxy population of a cosmological box.

5.4 Caveats

Star formation happens throughout the galaxy, and our assumption that all gas needs to be kicked from $r = 0$ means that we overestimate to some extent the energy needed to

eject the gas completely from the halo. Furthermore, simply heating the gas to the virial temperature via SN is probably not enough to prevent all further star formation: the gas will buoyantly rise and then rain back down onto the disk as it cools. The specifics of this gas cycle can only really be teased out from numerical simulations that include all the relevant processes; however, results are still dependant on subgrid models of stellar feedback and resolution. Therefore there are still large uncertainties in the amount of gas that actually re-accretes onto a galaxy as not all simulations can include all of the potentially important physics such as magnetic fields, thermal conduction, and cosmic rays (Armillotta et al. 2016).

Our model assumes that if there were no stellar feedback, the cosmic fraction of baryons would settle into a cold disk of gas and stars. This is not necessarily the case as environment, mergers, and a variety of other cosmic mechanisms can disrupt this process. Indeed, both hydrodynamical simulation and semi-analytic models (Nelson et al. 2016; Mitchell et al. 2018) predict that a significant fraction of the baryons do not accrete in the first place, and observations indicate that some gas is shocked and remains hot. Since galaxies form hierarchically in Λ CDM, the actual amount of baryons that are needed to be removed from the cold disk of gas and stars is almost certainly less than what we have assumed in this paper as it is easier to eject baryons from one of the less massive progenitors. This makes our estimate of the required energy conservative. These processes may also introduce a mass dependence to the required feedback energy that our model does not account for.

“Missing baryons” may also be explained by heating the gas to a temperature that is not currently accessible by observations. This is not necessarily given by T_{vir} , so one

⁷ This mass function was computed with HMFcalc (Murray et al. 2013).

could replace T_{vir} in Equation 8 with a fixed temperature, changing the mass dependence in the equation.

We have completely neglected other forms of feedback related to star formation such as photoionization, radiation pressure, cosmic rays, or stellar winds. It is known that the energy input from stars in the form of radiation is roughly two orders of magnitude higher than the mechanical input from SN (e.g. Dalla Vecchia & Schaye 2008; Hopkins et al. 2014). Simulations have shown that this radiation or even earlier stellar feedback in the form of winds can help regulate galaxy growth (Hopkins et al. 2014). The scalings presented here will continue to hold as long as the feedback energy scales linearly with M_* . If, however, any of these processes are related to the mass of the galaxy, the predicted slope for the M_*/M_{halo} relation will cease to be 5/3. As noted above, it may be that “preventative feedback” may be more effective at lower masses which could decrease the slope of the relation.

We have assumed that once an NFW cusp has been destroyed by feedback it will not reform. If it did, energy would have to be supplied continuously to maintain the core, which would significantly increase the required feedback efficiency for a given star formation rate. It is possible for mergers to recreate a cusp, but it has been shown that a core can be recreated even after the merger (e.g. Tollet et al. 2016). Galaxies likely evolve through a cyclic pattern of having cores and cusps depending on their ratio of M_*/M_{halo} (Tollet et al. 2016). Thus, while cusps tend to form again in dark matter-only simulations (Laporte & Peñarrubia 2015), this may not necessarily be the case when full hydrodynamics is considered. In particular, it is during mergers that cusps tend to form again in N-body only simulations, but mergers also trigger star formation which drives the outflows that may oppose this transformation.

Finally, all of our conclusions are subject to any selection effects that may be present in the SPARC sample. This sample is representative of the the overall galaxy population in most key properties (Lelli et al. 2016), but is neither complete nor volume limited. We only consider late-type galaxies, which may in part cause our derived slope for the M_*/M_{halo} relation to systematically disagree with literature relations (Moster et al. 2013; Behroozi et al. 2013). Performing these same experiments with data sets which are either more or less representative or compiled in a more or less homogeneous fashion may lead to different results.

Given these uncertainties, we do not intend our analysis to prove that SN energy couples efficiently to the gas. We have however demonstrated that were this the case, this energy would be sufficient to create cores and produce rotation curves that match the SPARC sample. This is consistent with other results from the literature that present similar findings (Katz et al. 2017; Santos-Santos et al. 2018; Tollet et al. 2016).

6 CONCLUSION

We have calculated the fraction of “missing baryons” in 147 galaxies from the SPARC database, using empirically estimated halo masses from rotation curve fits for two different halo models: NFW and DC14 (see Katz et al. 2017). Our main results are as follows:

- We confirm that galaxy formation is a globally inefficient process. The observed fraction of baryons present in the cold disk is in general much smaller than the cosmic baryon fraction. This fraction scales weakly with the virial mass of the galaxy such that $f_d \propto M_{\text{vir}}^{0.16}$, although there is significant scatter about this relation. Likewise, the fraction of baryonic mass comprised of stars scales strongly with mass; the most massive galaxies in our sample are completely dominated by stars. At $M_{\text{vir}} \sim 10^{11.1}$, roughly 50% of the observed baryonic content is in cold gas and the other 50% is in stars.

- When comparing the energy required to heat the “missing baryons” to the virial temperature versus eject them from the halo, we find that far less energy is required for the former. For SN feedback to regulate the heating, $\lesssim 10\%$ of the total SN energy available needs to couple to the gas (dependent on the stellar IMF). We find that a constant coupling efficiency is sufficient to explain the “missing baryons” for late-type spiral galaxies in the mass range $10^9 < M_{\text{vir}}/M_{\odot} < 10^{12}$ when haloes are modelled with a DC14 profile. This then sets the slope of the M_*/M_{vir} relation to be slightly less than 5/3 due to the weak scaling of f_d with M_{vir} . However, there is typically not enough SN energy to eject all of the missing baryons from the halo.

- When comparing the energy required to restructure the halo from a primordial NFW profile to the DC14 form, we find that there is always more energy available from SN feedback than required for the transformation. We find that there is no mass dependence in the SN coupling efficiency required to create cores and that the magnitude of this efficiency is very similar to what is required to heat the “missing baryons”. In contrast, there is a mass dependency in the efficiency required to erase the halo transformation for systems that exhibit contraction. This may indicate that halo restructuring is dependent on quantities other than stellar mass such as halo mass, formation redshift, or star formation history.

- We take a cosmic census of the baryons that should be associated with late-type galaxies, finding that $\sim 86\%$ of the total baryonic content is likely to be in a hot halo surrounding the galaxy, and the remaining 14% split equally between stars and gas. In order for our predictions to be confirmed, future X-ray or kinetic Sunyaev-Zeldovich observations will have to accurately measure the masses in hot gas surrounding these local galaxies.

ACKNOWLEDGEMENTS

We thank the anonymous referee for their suggestions that improved the manuscript. H.K. thanks the Beecroft fellowship, the Nicholas Kurti Junior Fellowship, and Brasenose College. H.D. is supported by St John’s College, Oxford. ADC acknowledges financial support from a Marie Skłodowska-Curie Individual Fellowship grant, H2020-MSCA-IF-2016, Grant agreement 748213, DIGESTIVO.

REFERENCES

Anderson M. E., Bregman J. N., 2011, *ApJ*, **737**, 22

- Anderson M. E., Bregman J. N., Dai X., 2013, *ApJ*, **762**, 106
- Armillotta L., Fraternali F., Marinacci F., 2016, *MNRAS*, **462**, 4157
- Babul A., Rees M. J., 1992, *MNRAS*, **255**, 346
- Behroozi P. S., Wechsler R. H., Conroy C., 2013, *ApJ*, **770**, 57
- Bernardi M., Meert A., Sheth R. K., Vikram V., Huertas-Company M., Mei S., Shankar F., 2013, *MNRAS*, **436**, 697
- Blumenthal G. R., Faber S. M., Flores R., Primack J. R., 1986, *ApJ*, **301**, 27
- Bower R. G., Benson A. J., Malbon R., Helly J. C., Frenk C. S., Baugh C. M., Cole S., Lacey C. G., 2006, *MNRAS*, **370**, 645
- Bradford J. D., Geha M. C., Blanton M. R., 2015, *ApJ*, **809**, 146
- Bregman J. N., Alves G. C., Miller M. J., Hodges-Kluck E., 2015, *Journal of Astronomical Telescopes, Instruments, and Systems*, **1**, 045003
- Bregman J. N., Anderson M. E., Miller M. J., Hodges-Kluck E., Dai X., Li J.-T., Li Y., Qu Z., 2018, preprint, ([arXiv:1803.08963](https://arxiv.org/abs/1803.08963))
- Breitschwerdt D., McKenzie J. F., Voelk H. J., 1991, *A&A*, **245**, 79
- Brook C. B., Di Cintio A., 2015, *MNRAS*, **453**, 2133
- Brook C. B., Stinson G., Gibson B. K., Wadsley J., Quinn T., 2012, *MNRAS*, **424**, 1275
- Brook C. B., Stinson G., Gibson B. K., Shen S., Macciò A. V., Obreja A., Wadsley J., Quinn T., 2014, *MNRAS*, **443**, 3809
- Cen R., Ostriker J. P., 1999, *ApJ*, **514**, 1
- Chabrier G., 2003, *PASP*, **115**, 763
- Chabrier G., Baraffe I., Allard F., Hauschildt P. H., 2005, *ArXiv Astrophysics e-prints*,
- Chan T. K., Kereš D., Oñorbe J., Hopkins P. F., Muratov A. L., Faucher-Giguère C. A., Quataert E., 2015, *Mon. Not. Roy. Astron. Soc.*, **454**, 2981
- Christensen C. R., Davé R., Governato F., Pontzen A., Brooks A., Munshi F., Quinn T., Wadsley J., 2016, *ApJ*, **824**, 57
- Concas A., Popesso P., Brusa M., Mainieri V., Erfanianfar G., Morselli L., 2017, *A&A*, **606**, A36
- Costa T., Sijacki D., Haehnelt M. G., 2014, *MNRAS*, **444**, 2355
- Cowie L. L., McKee C. F., Ostriker J. P., 1981, *ApJ*, **247**, 908
- Curtis M., Sijacki D., 2016, *MNRAS*,
- Dalla Vecchia C., Schaye J., 2008, *Monthly Notices of the Royal Astronomical Society*, **387**, 1431
- Danforth C. W., Shull J. M., 2005, *ApJ*, **624**, 555
- Dekel A., Silk J., 1986, *ApJ*, **303**, 39
- Dekel A., Ishai G., Dutton A. A., Macciò A. V., 2017, *MNRAS*, **468**, 1005
- Di Cintio A., Brook C. B., Macciò A. V., Stinson G. S., Knebe A., Dutton A. A., Wadsley J., 2014a, *MNRAS*, **437**, 415
- Di Cintio A., Brook C. B., Dutton A. A., Macciò A. V., Stinson G. S., Knebe A., 2014b, *MNRAS*, **441**, 2986
- Di Cintio A., Tremmel M., Governato F., Pontzen A., Zavala J., Bastidas Fry A., Brooks A., Vogelsberger M., 2017, *MNRAS*, **469**, 2845
- Dubois Y., et al., 2014, *MNRAS*, **444**, 1453
- Dutton A. A., Macciò A. V., 2014, *MNRAS*, **441**, 3359
- Dutton A. A., et al., 2011, *MNRAS*, **416**, 322
- Efstathiou G., 1992, *MNRAS*, **256**, 43P
- Efstathiou G., 2000, *MNRAS*, **317**, 697
- Elbaz D., et al., 2007, *A&A*, **468**, 33
- Fall S. M., Efstathiou G., 1980, *MNRAS*, **193**, 189
- Fischler M. A., Bolles R. C., 1981, *Commun. ACM*, **24**, 381
- Fukugita M., Hogan C. J., Peebles P. J. E., 1998, *ApJ*, **503**, 518
- Gentry E. S., Krumholz M. R., Dekel A., Madau P., 2017, *MNRAS*, **465**, 2471
- Giodini S., et al., 2009, *ApJ*, **703**, 982
- Gnedin N. Y., 2000, *ApJ*, **542**, 535
- Gnedin O. Y., Kravtsov A. V., Klypin A. A., Nagai D., 2004, *ApJ*, **616**, 16
- Gonzalez A. H., Sivanandam S., Zabludoff A. I., Zaritsky D., 2013, *ApJ*, **778**, 14
- Hernquist L., 1990, *ApJ*, **356**, 359
- Hopkins P. F., Kereš D., Murray N., Quataert E., Hernquist L., 2012, *MNRAS*, **427**, 968
- Hopkins P. F., Kereš D., Oñorbe J., Faucher-Giguère C.-A., Quataert E., Murray N., Bullock J. S., 2014, *MNRAS*, **445**, 581
- Hopkins P. F., et al., 2017, preprint, ([arXiv:1702.06148](https://arxiv.org/abs/1702.06148))
- Karim A., et al., 2011, *ApJ*, **730**, 61
- Katz H., McGaugh S. S., Sellwood J. A., de Blok W. J. G., 2014, *MNRAS*, **439**, 1897
- Katz H., Lelli F., McGaugh S. S., Di Cintio A., Brook C. B., Schombert J. M., 2017, *MNRAS*, **466**, 1648
- Kereš D., Katz N., Weinberg D. H., Davé R., 2005, *MNRAS*, **363**, 2
- King A., 2003, *ApJ*, **596**, L27
- Laporte C. F. P., Peñarrubia J., 2015, *MNRAS*, **449**, L90
- Lelli F., Verheijen M., Fraternali F., 2014, *A&A*, **566**, A71
- Lelli F., McGaugh S. S., Schombert J. M., 2016, preprint, ([arXiv:1606.09251](https://arxiv.org/abs/1606.09251))
- Li C., White S. D. M., 2009, *MNRAS*, **398**, 2177
- Li J.-T., Bregman J. N., Wang Q. D., Crain R. A., Anderson M. E., 2018, preprint, ([arXiv:1802.09453](https://arxiv.org/abs/1802.09453))
- Macciò A. V., Dutton A. A., van den Bosch F. C., 2008, *MNRAS*, **391**, 1940
- Marinacci F., Binney J., Fraternali F., Nipoti C., Ciotti L., Londrillo P., 2010, *MNRAS*, **404**, 1464
- Martizzi D., Teyssier R., Moore B., 2013, *MNRAS*, **432**, 1947
- Mathews W. G., Baker J. C., 1971, *ApJ*, **170**, 241
- Maxwell A. J., Wadsley J., Couchman H. M. P., 2015, *ApJ*, **806**, 229
- McGaugh S. S., Schombert J. M., 2014, *AJ*, **148**, 77
- McGaugh S. S., Schombert J. M., de Blok W. J. G., Zagursky M. J., 2010, *ApJ*, **708**, L14
- McKee C. F., Ostriker J. P., 1977, *ApJ*, **218**, 148
- Miller M. J., Bregman J. N., 2015, *ApJ*, **800**, 14
- Mitchell P., Blaizot J., Devriendt J., Kimm T., Michel-Dansac L., Rosdahl J., Slyz A., 2017, preprint, ([arXiv:1710.03765](https://arxiv.org/abs/1710.03765))
- Mitchell P. D., et al., 2018, *MNRAS*, **474**, 492
- Moster B. P., Naab T., White S. D. M., 2013, *MNRAS*, **428**, 3121
- Moster B. P., Naab T., White S. D. M., 2017, preprint, ([arXiv:1705.05373](https://arxiv.org/abs/1705.05373))
- Murray S. G., Power C., Robotham A. S. G., 2013, *Astronomy and Computing*, **3**, 23
- Navarro J. F., Eke V. R., Frenk C. S., 1996a, *MNRAS*, **283**, L72
- Navarro J. F., Frenk C. S., White S. D. M., 1996b, *ApJ*, **462**, 563
- Nelson D., Genel S., Pillepich A., Vogelsberger M., Springel V., Hernquist L., 2016, *MNRAS*, **460**, 2881
- Okamoto T., Gao L., Theuns T., 2008, *MNRAS*, **390**, 920
- Papastergis E., Cattaneo A., Huang S., Giovanelli R., Haynes M. P., 2012, *ApJ*, **759**, 138
- Peñarrubia J., Pontzen A., Walker M. G., Koposov S. E., 2012, *ApJ*, **759**, L42
- Pedregosa F., et al., 2011, *Journal of Machine Learning Research*, **12**, 2825
- Planck Collaboration et al., 2015, preprint, ([arXiv:1502.01589](https://arxiv.org/abs/1502.01589))
- Pontzen A., Governato F., 2012, *MNRAS*, **421**, 3464
- Puchwein E., Sijacki D., Springel V., 2008, *ApJ*, **687**, L53
- Read J. I., Gilmore G., 2005, *MNRAS*, **356**, 107
- Read J. I., Agertz O., Collins M. L. M., 2016a, *MNRAS*, **459**, 2573
- Read J. I., Agertz O., Collins M. L. M., 2016b, *Mon. Not. Roy. Astron. Soc.*, **459**, 2573
- Rogers H., Pittard J. M., 2013, *MNRAS*, **431**, 1337
- Salpeter E. E., 1955, *ApJ*, **121**, 161
- Santos-Santos I. M., Di Cintio A., Brook C. B., Macciò A., Dutton A., Domínguez-Tenreiro R., 2018, *MNRAS*, **473**, 4392

- Sawala T., et al., 2016, *Mon. Not. Roy. Astron. Soc.*, 457, 1931
 Schaye J., et al., 2015, *MNRAS*, 446, 521
 Sedov L. I., 1959, *Similarity and Dimensional Methods in Mechanics*
 Shull J. M., Smith B. D., Danforth C. W., 2012, *ApJ*, 759, 23
 Silk J., Rees M. J., 1998, *A&A*, 331, L1
 Spergel D. N., et al., 2003, *ApJS*, 148, 175
 Spergel D. N., et al., 2007, *ApJS*, 170, 377
 Stinson G. S., Brook C., Macciò A. V., Wadsley J., Quinn T. R., Couchman H. M. P., 2013, *MNRAS*, 428, 129
 Tanimura H., Hinshaw G., McCarthy I. G., Van Waerbeke L., Ma Y.-Z., Mead A., Hojjati A., Tröster T., 2017, preprint, ([arXiv:1709.05024](https://arxiv.org/abs/1709.05024))
 Taylor G., 1950, *Proceedings of the Royal Society of London Series A*, 201, 159
 Tollet E., et al., 2016, *MNRAS*, 456, 3542
 Tumlinson J., Peebles M. S., Werk J. K., 2017, *ARA&A*, 55, 389
 Veilleux S., Cecil G., Bland-Hawthorn J., 2005, *ARA&A*, 43, 769
 Vogelsberger M., et al., 2014, *MNRAS*, 444, 1518
 Walch S., Naab T., 2015, *MNRAS*, 451, 2757
 White S. D. M., Frenk C. S., 1991, *ApJ*, 379, 52
 White S. D. M., Rees M. J., 1978, *MNRAS*, 183, 341
 Yepes G., Kates R., Khokhlov A., Klypin A., 1997, *Monthly Notices of the Royal Astronomical Society*, 284, 235
 de Graaff A., Cai Y.-C., Heymans C., Peacock J. A., 2017, preprint, ([arXiv:1709.10378](https://arxiv.org/abs/1709.10378))

APPENDIX A: ANALYTIC EXPRESSIONS FOR THE (α, β, γ) PROFILE

The (α, β, γ) profile (Hernquist 1990) is defined by

$$\rho(r) = \frac{\rho_s}{\left(\frac{r}{r_s}\right)^\gamma \left(1 + \left(\frac{r}{r_s}\right)^\alpha\right)^{\frac{\beta-\gamma}{\alpha}}}, \quad (\text{A1})$$

where r_s and ρ_s are the scale radius and scale density of the halo respectively. At small r the density has a logarithmic slope of γ , while at large r it falls off as $\rho \propto r^{-\beta}$. α marks the transition strength between these two regimes. In general, the power-law slope of the profile can be derived as

$$s(r) = -\frac{d \log \rho}{d \log r} = -\frac{\gamma + \beta \left(\frac{r}{r_s}\right)^\alpha}{1 + \left(\frac{r}{r_s}\right)^\alpha}. \quad (\text{A2})$$

To solve for the potential,

$$\Phi(r) = -4\pi G \left(\frac{1}{r} \int_0^r \rho(r') r'^2 dr' + \int_r^\infty \rho(r') r' dr' \right), \quad (\text{A3})$$

we make the following assumptions: $\alpha > 0$, $0 < \gamma < 2$, $\beta > 2$, $\rho_s > 0$, and $r_s > 0$. Evaluating these integrals we find two cases:

$$\Phi(r) = \begin{cases} -4\pi G \rho_s (A_1[r] + A_2[r]), & \text{if } r > 0 \\ \frac{-4\pi G \rho_s r_s^2 \Gamma\left[\frac{\beta-2}{\alpha}\right] \Gamma\left[\frac{2-\gamma}{\alpha}\right]}{\alpha \Gamma\left[\frac{\beta-\gamma}{\alpha}\right]}, & \text{if } r = 0 \end{cases} \quad (\text{A4})$$

where

$$A_1(r) = \frac{-r^{2-\gamma} r_s^\gamma {}_2F_1\left[\frac{3-\gamma}{\alpha}, \frac{\beta-\gamma}{\alpha}; \frac{3+\alpha-\gamma}{\alpha}; -\left(\frac{r}{r_s}\right)^\alpha\right]}{\gamma - 3} \quad (\text{A5})$$

$$A_2(r) = \frac{r^{2-\beta} r_s^\beta {}_2F_1\left[\frac{\beta-2}{\alpha}, \frac{\beta-\gamma}{\alpha}; \frac{\alpha+\beta-2}{\alpha}; -\left(\frac{r}{r_s}\right)^\alpha\right]}{\beta - 2}. \quad (\text{A6})$$

Here, ${}_2F_1[a, b; c; z]$ is the Gaussian or ordinary hypergeometric function and $\Gamma[x]$ is the gamma function.

Our assumptions on α , β , & γ were made so that

$$\lim_{r \rightarrow 0} \frac{1}{r} \int_0^r \rho(r') r'^2 dr' = 0 \quad (\text{A7})$$

and

$$\lim_{r \rightarrow \infty} \Phi(r) = 0. \quad (\text{A8})$$

These minor restrictions encompass the wide range of α , β , & γ that real galaxies are expected to exhibit and do not limit our ability to fit rotation curves (Di Cintio et al. 2014b; Katz et al. 2017).

We can now calculate the escape speed, V_{esc} , at any chosen radius:

$$V_{\text{esc}} = \sqrt{2|\Phi(r)|}. \quad (\text{A9})$$

The mass distribution within the galaxy is given by

$$M(r) = 4\pi \rho_s \int_0^r \frac{r'^2}{\left(\frac{r'}{r_s}\right)^\gamma \left(1 + \left(\frac{r'}{r_s}\right)^\alpha\right)^{\frac{\beta-\gamma}{\alpha}}} dr'. \quad (\text{A10})$$

Using our previous solution of this integral in calculating the potential:

$$M(r) = 4\pi \rho_s r A_1[r]. \quad (\text{A11})$$

This defines the circular velocity, $V_c(r)$, at any given radius by

$$V_c(r) = \sqrt{4\pi G \rho_s A_1[r]}. \quad (\text{A12})$$

These equations have all been given in terms of ρ_s and r_s . We can reformulate them in terms of concentration c and virial velocity V_{vir} by using

$$r_s = \frac{r_{-2}}{\left(\frac{2-\gamma}{\beta-2}\right)^{1/\alpha}}, \quad (\text{A13})$$

where

$$r_{-2} = \frac{R_{\text{vir}}}{c}. \quad (\text{A14})$$

Here, we define the concentration as R_{vir} divided by the radius, r_{-2} , where the logarithmic slope of the profile reaches the value of -2 . In the NFW model, this corresponds to r_s , in a general (α, β, γ) model, r_{-2} is given by Equation A13. Hence,

$$r_s = \frac{R_{\text{vir}}}{c \left(\frac{2-\gamma}{\beta-2}\right)^{1/\alpha}}. \quad (\text{A15})$$

We can find ρ_s by inverting Equation A10 and evaluating at R_{vir} . For this, we have

$$\rho_s = \frac{M_{\text{vir}}}{4\pi R_{\text{vir}} A_1[R_{\text{vir}}]}. \quad (\text{A16})$$

We can then place this in the context of V_{vir} by using

$$R_{\text{vir}} = \left(\frac{M_{\text{vir}}}{\frac{4\pi\Delta}{3} \rho_{\text{crit}}} \right)^{1/3} \quad (\text{A17})$$

and

$$M_{\text{vir}} = \frac{V_{\text{vir}}^3}{\sqrt{\frac{\Delta}{2} G H_0}}, \quad (\text{A18})$$

so

$$R_{\text{vir}} = \frac{V_{\text{vir}}}{H_0 \sqrt{\frac{\Delta}{2}}}. \quad (\text{A19})$$

Here, Δ is the over-density with respect to the critical density, ρ_{crit} at which a halo is considered virialized, G is the gravitational constant, and H_0 is the Hubble constant.

Substituting in for A_1 and ρ_s , we find

$$A_1(r) = \frac{-r^{2-\gamma} {}_2F_1 \left[\frac{3-\gamma}{\alpha}, \frac{\beta-\gamma}{\alpha}; \frac{3+\alpha-\gamma}{\alpha}; -\left(\frac{r\sqrt{\frac{\Delta}{2}}H_0c}{V_{\text{vir}}} \right)^\alpha \right]}{\left(\frac{V_{\text{vir}}}{\sqrt{\frac{\Delta}{2}}H_0c} \right)^{-\gamma} (\gamma-3)} \quad (\text{A20})$$

and

$$\rho_s = \frac{V_{\text{vir}}^2}{4\pi G A_1 \left[\frac{V_{\text{vir}}}{\sqrt{\frac{\Delta}{2}}H_0c} \right]}. \quad (\text{A21})$$

We can now calculate Φ , $M(r)$, and $V_c(r)$ solely from c and V_{vir} without the use of numerical integrals.

In this work, when we consider the ejection model, we will assume that all baryons need to be ejected from the centre of the halo. While it is unlikely that all of the gas is at $r = 0$, stars tend to form at the centres of galaxies in the highest density gas, so it is likely that the outflowing gas originates at $r \ll R_{\text{vir}}$. While this may be overestimating the true V_{esc} of a small parcel of gas, we will assume later that the rest of the baryonic matter is evenly spread throughout the halo, which causes us to underestimate V_{esc} from the centre. Although simple, our assumptions are therefore not obviously systematically biased.

We now have the means to use an analytic set of functions to calculate V_{esc} as a function of c , V_{vir} , α , β , and γ . Putting this all together, we find

$$V_{\text{esc}}(r=0) = \sqrt{2 \left| \frac{(\gamma-3)V_{\text{vir}}^2 \left(\frac{1-\gamma}{\beta-2} \right)^{(2-\gamma)/\alpha} \Gamma\left(\frac{\beta-2}{\alpha}\right) \Gamma\left(\frac{2-\gamma}{\alpha}\right)}{\alpha c^{2-\gamma} \Gamma\left(\frac{\beta-\gamma}{\alpha}\right) {}_2F_1 \left[\frac{3-\gamma}{\alpha}, \frac{\beta-\gamma}{\alpha}; \frac{3+\alpha-\gamma}{\alpha}; -c \left(\frac{1-\gamma}{\beta-2} \right) \right]} \right|}. \quad (\text{A22})$$

For the NFW halo ($\alpha = 1$, $\beta = 3$, $\gamma = 1$), these equations simplify considerably. In this special case, we find that

$$\Phi_{\text{NFW}}(r=0) = \frac{-cV_{\text{vir}}^2}{\log(1+c) - \frac{c}{1+c}}. \quad (\text{A23})$$

Therefore

$$V_{\text{esc,NFW}} = \sqrt{2 \left| \frac{-cV_{\text{vir}}^2}{\log(1+c) - \frac{c}{1+c}} \right|}. \quad (\text{A24})$$

To demonstrate the difference between the two halo models, in Figure A1 we compare V_{esc} for the NFW and DC14 models as a function of halo mass for galaxies that fall on the M_*/M_{halo} relation as given in [Moster et al. \(2013\)](#) and the $M_{\text{vir}} - c$ relation as given by [Dutton & Macciò \(2014\)](#). The maximum difference in V_{esc} for these galaxies is $\sim 7\%$. Since we expect galaxies to fall close to these relations, it is reasonable to assert that for both of these two halo models, $V_{\text{esc}} \propto V_{\text{vir}} \propto M_{\text{vir}}^{1/3}$. This scaling can be seen in Figure A1.

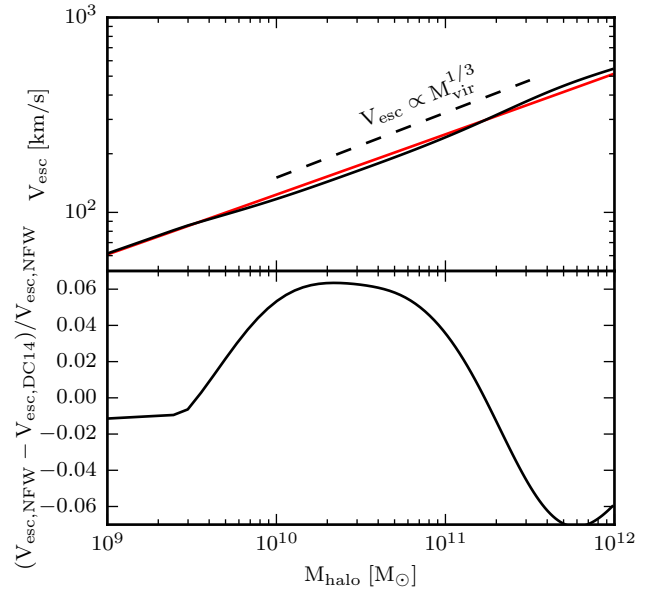


Figure A1. (Top) Comparison of the escape velocity of an NFW halo (red) versus a DC14 halo (black) with properties that fall on the M_*/M_{halo} relation as given in [Moster et al. \(2013\)](#) and the $M_{\text{vir}} - c$ relation as given by [Dutton & Macciò \(2014\)](#), as a function of halo mass. (Bottom) Percentage difference between the NFW and DC14 halo models.